Anti-Earthquake Measures for Embankment on a Weak Ground

by

Hiroshi Uezawa[I] and Makoto Nasu[II]

Synopsis

The present paper is a report on the results of a series of studies carried out to work out protective measures for sandy embankment which is highly vulnerable to heavy shocks of earthquake. The contents consist of the classification of types of embankment failure under earthquake, influence of rain prior to earthquake, measurement of dynamic pore-water pressure in heavy earthquake, field survey of a failed embankment and the failure tests of model embankment on a large-size shaking table.

1. Introduction

The failures of embankment due to earthquake are classified into the following four types: slope slip (type I), slope failure (type II), longitudinal crack (type III) and subsidence (type IV), (Fig.1). At the tip of collapsed earth, a mud flow oozing out of the slip plane is invariably recognized, testifying that the sandy soil has been liquefied. Slope slip is observed most frequently in new embankment, slope surface layer of which has been finished relatively loose on account of difficulty to roll, and the slip is induced by the rise of pore-water pressure in slope surface layer. The rise of pore-water pressure by the rain prior to earthquake is explained by calculation and measurement.
We successfully measured amount of rise of dynamic pore-water pressure in situ caused by the Tokachioki earthquake (May 16, 1968; Magnitude 7.8). Relative density of filled sand was less than 0.5 and the bottom of embankment was found completely saturated with water where slope failure had occured on a large scale. Slope failure should have been caused by rise of pore-water pressure at the bottom of embankment and subsidence, by flow aside of weak ground. This process was recognized also by the experiments on a large-size shaking table. Experiments of anti-earthquake measures such as the method of filling gravel at the bottom of embankment, embedding tensional material, and the sheet piling method were carried out and were proposed the respective measures anainst the four types failures.

2. Influence of the rain prior to earthquake

It had rained reaching 120-150mm since a few days prior to the Tokachioki earthquake, and the pore-water pressure might had been increased, since infiltrated water must had been collected in loose slope surface layer on compacted core of embankment. The rise of pore-water pressure due

---

I Chief Researcher, Soil Mechanics Laboratory, Railway Technical Research Institute, Japanese National Railways, Kunitachi Tokyo, Japan

II same above

to rain can be calculated as follows (see Fig.4):

if L = length of well compacted impervious layer parallel to slope
θ = slope angle
n = effective porosity of slope surface layer
R = rain rate
K = coefficient of permeability
h = the height of water level,

the total quantity of water that enters the slope surface layer is $R \cdot L \cdot \cos\theta \cdot dt$. The quantity that leaves it is $K \cdot \sin\theta \cdot \cos\theta \cdot h \cdot dt$. Therefore, the quantity that remains in the slope surface layer is

$$dh \cdot L \cdot \cos\theta \cdot n = R \cdot L \cdot \cos\theta \cdot dt - K \cdot \sin\theta \cdot \cos\theta \cdot h \cdot dt \quad \cdots\cdots\cdots (1)$$

By integrating Equation (1), we obtain the height of water level, h. The result is shown in Fig.4. The height of water level is estimated as 0.6m to 0.9m just before the earthquake. An example of pore-water pressure measured on the Shinkansen is shown in Fig.5. The pore-water pressure rises up to the height of 0.4m to 0.9m after each rainfall. If an earthquake should happened in this case, the further rise of pore-water pressure would caused a slope slip of embankment.

3. Measurement of dynamic pore-water pressure in heavy earthquake

Measurement of a rise in the pore-water pressure due to earthquake have seldom been executed in the world. In the Tokachioki earthquake we successfully measured the rise in the pore-water pressure in a weak ground beneath railway embankment as caused by the earthquake shocks (Fig.6). The behavior of the pore-water pressure was different depending on each measuring point; the maximum rise of 2.6m was registered, which is equivalent to 20% of the effective overburden pressure.

4. Field survey of a failed embankment

Fig.2 is a cross section through a embankment where type II failure occured on a large scale in the Niigata earthquake (June 16, 1964; Magnitude 7.5). The fill material of the embankment 7m high flowed far away over 100m toward the right direction. The right side of the embankment had rested on a weak soil layer 3m thick. Embankment failed but ground surface did not failed. Fill material is uniform sand with the uniformity coefficient U = 2.0 - 2.3, the effective grain size, D_{10} = 0.15 - 0.2mm. The void ratio was measured using undisturbed samples taken from the embankment which had been restored with the same material. The penetration resistance qc (kg/cm^2) was measured with the Dutch-type penetrometer and the water level at the bottom of the embankment was also measured. The relation between the value of qc (kg/cm^2) and the void ratio e is shown in Fig.3. If the value of qc at the bottom of embankment is $15kg/cm^2$ on an average, the void ratio may be about 0.85; consequently the relative density is calculated to be 0.47, when γ max = 0.976 and γ min = 0.709, γ max and γmin being the maximum and the minimum void ratio, respectively. The water table was located 0.7m to 1.4m above the original ground surface, showing that the bottom of embankment had been completely saturated. Thus it has

been revealed that the failed embankment was susceptible to be liquefied.

5. Failure test of embankment without countermeasure on a large-size shaking table

On a large-size shaking table (maximum loading capacity 100 tons, maximum output of vibrator 40 tons), a saturated weak ground 1m thick and a nonsaturated embankment 1.5m high upon it were built up (Fig.14). Fill material was sand with the uniformity coefficient U = 6.7, the effective grain size D_{10} = 0.03mm, e_{max} = 1.88 and e_{min} = 1.05. The relative density were 0.44 and 0.55 for the embankment and the ground, respectively. Sinusoidal vibrations of 7 HZ were given at 100 gals for the initial 10 seconds, then at 200 gals for 10 - 20 sec; 300 gals for the next 20 - 30 sec and continuously at 400 gals from the 30th second to the end of testing. The failure of an embankment with no protection provided on a weak ground was accompanied by a unique pattern of the pore-water pressure behavior (Fig.7～8); particulary at the core bottom of the embankment, the pressure showed a sudden increase in 20 seconds of vibration, the maximum value amounting to 95% of the effective overburden pressure. As for the pressures in the ground, a high value was registered, particularly beneath the toe of the slope, where the pore-water pressure in 10 seconds of vibration amounted to approximately the effective overburden pressure. The relation between the ratio of pore-water pressure to the effective overburden pressure and time is shown in Fig.8. This indicates that liquefaction occurs earlier beneath the toe of the slope, and later in the middle of the ground. Failures of types II, and III occured and development of a slip plane at the bottom of embankment was recognized. Type IV failure (subsidence) developed from the beginning of testing and toward the end it became conspicuous; this is attributable to the flow aside of the weak ground. In other experiment, failure of type I has been found to be the result of rain water collected in the slope surface layer of a filling which was finished relatively loose, the pore-water pressure there being increased through vibration and slope slip being caused thereby.

6. Failure test of embankment with countermeasure on the large-size shaking table

6.1 The method of filling gravel blanket under the embankment

Next, a series of experiments to work out the countermeasures are described. In the first place, the method of filling gravel under the embankment was tested (Fig.9). This method was effective in preventing a pore-water pressure rise at the bottom of embankment and accordingly the embankment remained stable with no failures of types II and III, except a minor subsidence observed. From the scratch of gravel remained on the inner side wall of the fill box of the shaking table, the blocks under both slopes of the embankment seemed to have slided aside, and central part of the embankment to have only subsided (Fig.9).

6.2 The method of embedding tensional material in the embankment

The effect of several tension members such as perforated pipes at the bottom of the embankment for drainage and reinforcement, steel rods with

retaining plates on both ends (Fig.10d), net at the bottom or within the whole embankment (Fig.10a,b), and Terre Armée (Reinforced earth, Fig.10c) developed in France have been examined. As there occured no serioud failure except subsidence, these methods have been found to be extremely effective. Tensile force acting on tensional material, for example, in the case of steel rods with retaining plates, is calculated as follows. Safety factor Fs against slide of the traingular block under slope is

$$Fs = \frac{P}{W \cdot K} \quad \cdots\cdots\cdots \quad (2)$$

where P = measured tensile force acting on tentional material
W = weight of triangular block (from the result of 6.1)
K = measured seismic coefficient

The result are shown in Fig.11. Safety factor Fs had been kept about 1.0 for 40 seconds till failure occured. As the measured values are balanced, so that Fs may be equal to 1, equation (2) may be seen as appropriate.

6.3 Sheet piling with tie rod

Subsidence develops from the beginning of vibration and towards the end it becomes conspicuous; this is attributable to flow aside of the weak ground. Sheet piling with tie rod (Fig.12) has been found most effective against subsidence. Tensile force acting on tie rods is analyzed as follows. Equilibrium of forces acting on sheet pile and tie rod is expressed by equation (3).

$$W \cdot K + D \cdot \frac{Wt}{B} \cdot \beta = P_1 + P_2 \quad \cdots\cdots\cdots \quad (3)$$

where
W = weight of assumed triangular sliding block
K = seismic coefficient
D = length of sheet pile
Wt = total weight of embankment
B = width of embankment base
β = coefficient of liquefaction (tentatively named)
$P_1 + P_2$ = total tensile force acting on upper and lower tie rods

Coefficient β is to reach 1.0 if weak ground is completely liquefied. Observed values β, K and $P_1 + P_2$ versus time are shown in Fig.(13). The value of β increases with time elapsing but does not exceed 1.0, so the equation (3) is considered to be reasonable.

7. Conclusion

Against slope slip which is caused by the rise of pore water pressure in loose slope surface layer, the method of making gravel mat on slope surface or inserting horizontally drainage pipes (6cm in dia., 3.6m long used in JNR) seems to be effective. The former increases the effective pressure and the latter decreases pore-water pressure, furthermore it reinforces the slope surface. Against slope failure and longitudinal crack

which are caused by the rise of pore water pressure at the bottom of embankment, the method of filling gravel blanket is effective for newly planned embankment. For existing embankment it is useful to insert perforated pipes at the bottom of embankment for drainage and reinforcement. Other methods such as counterweight embankment and toe retaining gravel berm which resist failure from outside are also useful. Against subsidence which is caused by flow aside of weak ground it is necessary to strengthen weak ground with gravel pile etc., for newly planned embankment. Counterweight embankment or sheet piling method is useful for existing embankment. It is desirable that most effective countermeasure will be employed after full grasp of the actual field conditions.

Acknowledgments

Much of the study is a part of the research conducted by the committee on Anti-Earthquake Design for Embankment (1968-1971), Japanese National Railways. The writers wish to express their gratitude to Dr. Shunzo Okamoto, Chairman of the Committee, Dr. Keizaburo Kubo, Chief Secretary, and other members, for their continuing guidance. The writers also wish to thank Dr. Takeichiro Ikehara, Deputy-Chief Engineer of JNR, Dr. Tatsuo Nishiki, Director of RTRI for their contribution to accomplishment of the large-size shaking table and Dr. Tadahiko Muromachi, Chief of Soil Mechanics Laboratory, for his consistent encouragement and advice to publish this paper.

References

Takeichiro Ikehara, (1972) "A Study on Damage of Railway Embankments due to the Tokachioki Earthquake", RTRI Report No.791.

Hiroshi Uezawa, Makoto Nasu and others, (1972) "An Experimental Study of Earthquake Resistance of Embankment by a Large-size Vibration Stand", RTRI Reports No.822, 823.

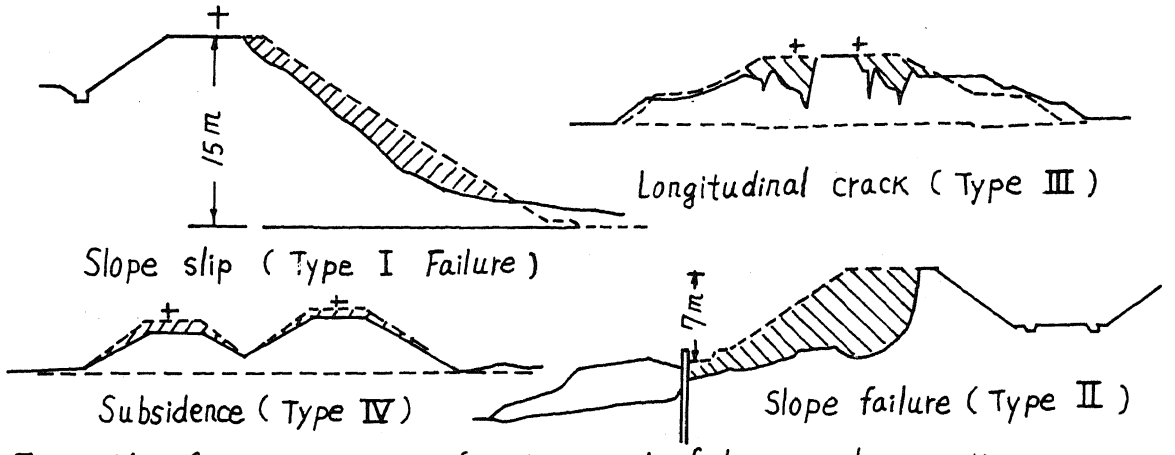

Fig.1 Classification of types of embankment failure under earthquake

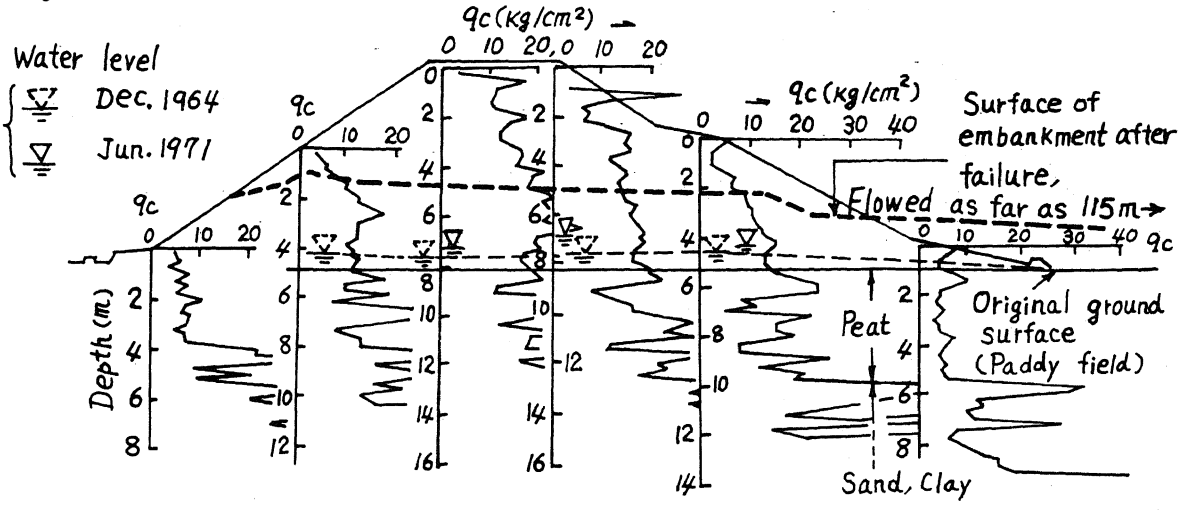

Fig.2 Dutch-type penetrometer records at a II type failed embankment measured after restored, at 221K180M on the Uetsu Line - Nishime -

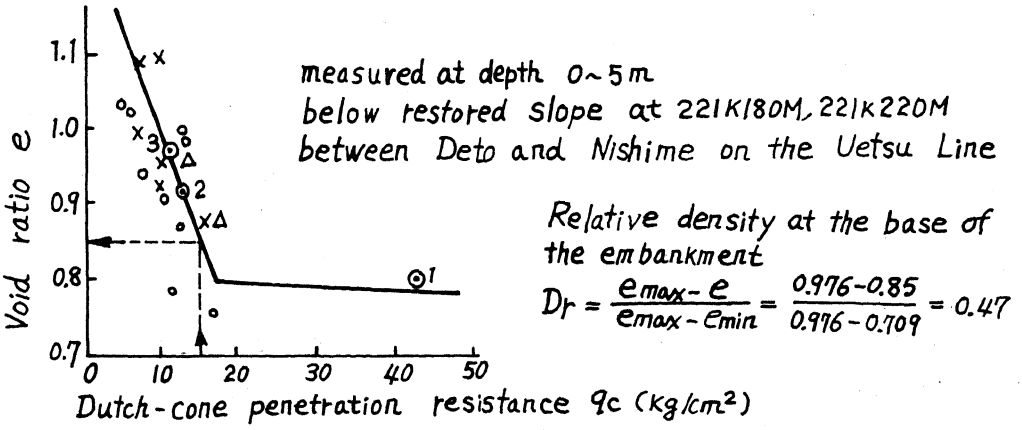

Fig.3 Relation between Dutch-cone penetration resistance and Void ratio of the sand on the spot

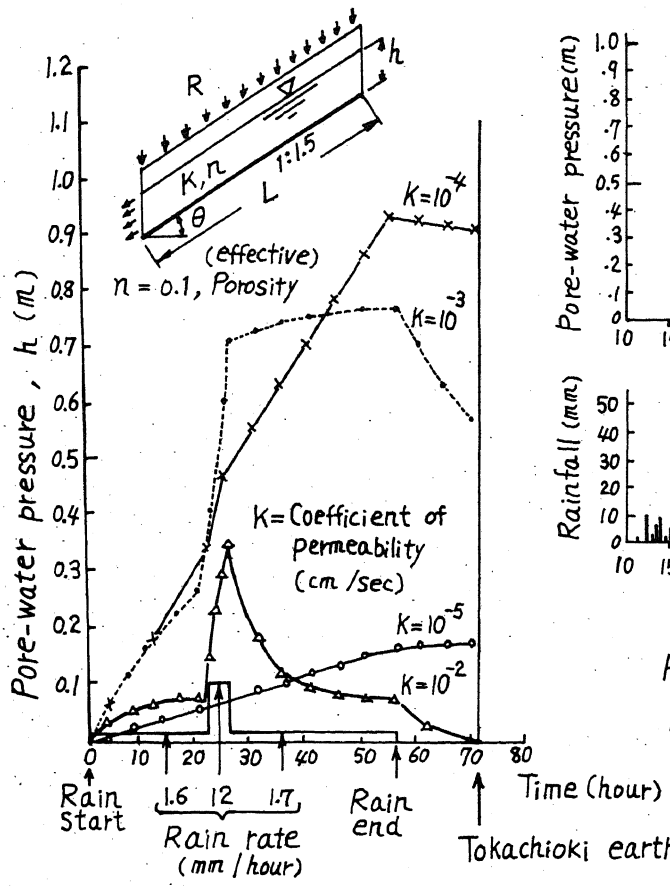

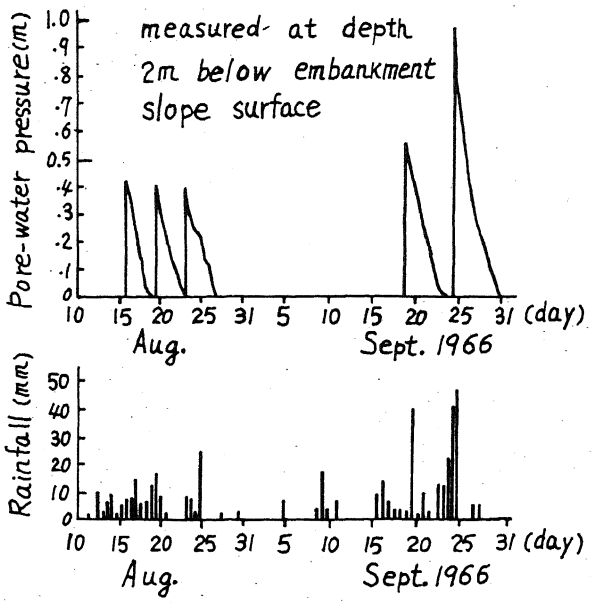

Fig. 5 Example of pore-water pressure measurement due to rain (at 314K200M on the Shinkansen)

Fig. 4 Calculated pore-water pressure due to rain (prior to the Tokachioki earthquake, 1968)

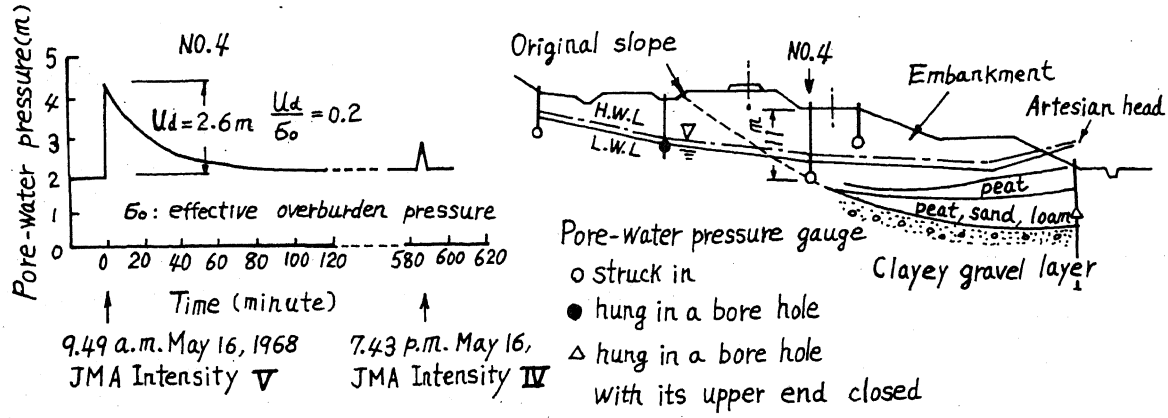

Fig. 6 Example of pore-water pressure measurement due to the Tokachioki earthquake, 1968 at a site between Mukaiyama and Misawa, Tohoku Trunk Line

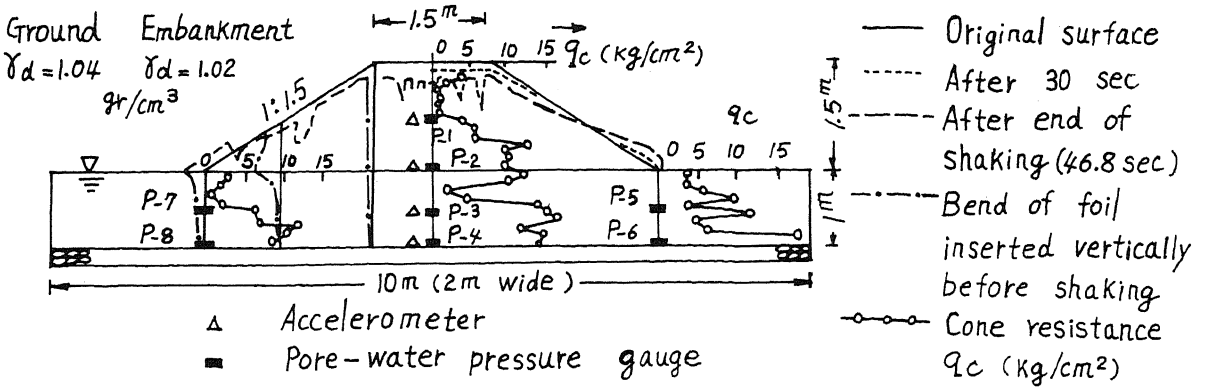

Fig. 7 Failure of model embankment without countermeasure

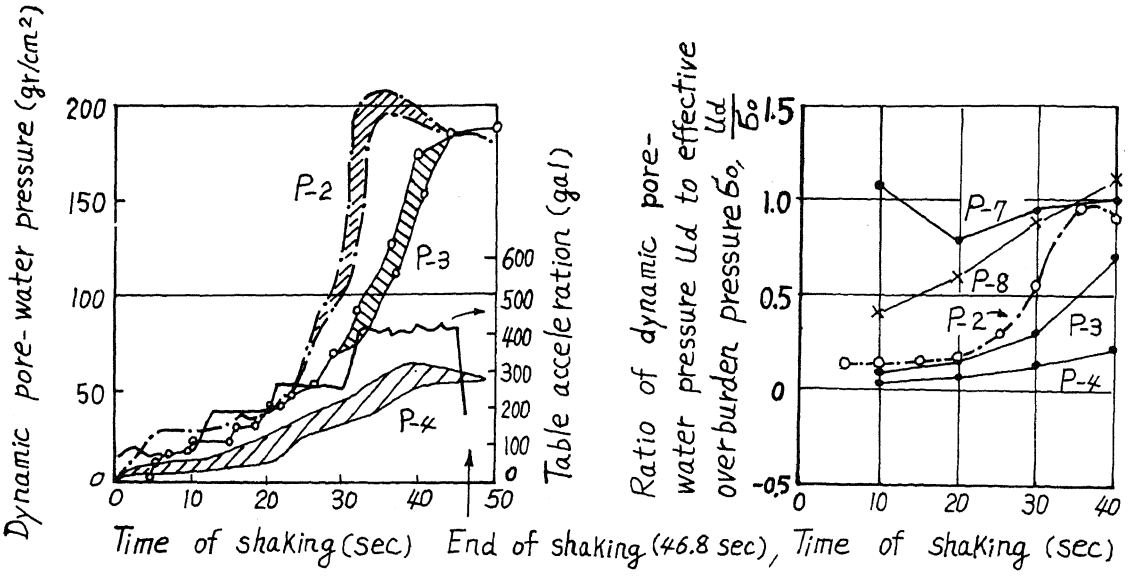

Fig. 8 Measurements of pore-water pressure (Embankment without countermeasure)

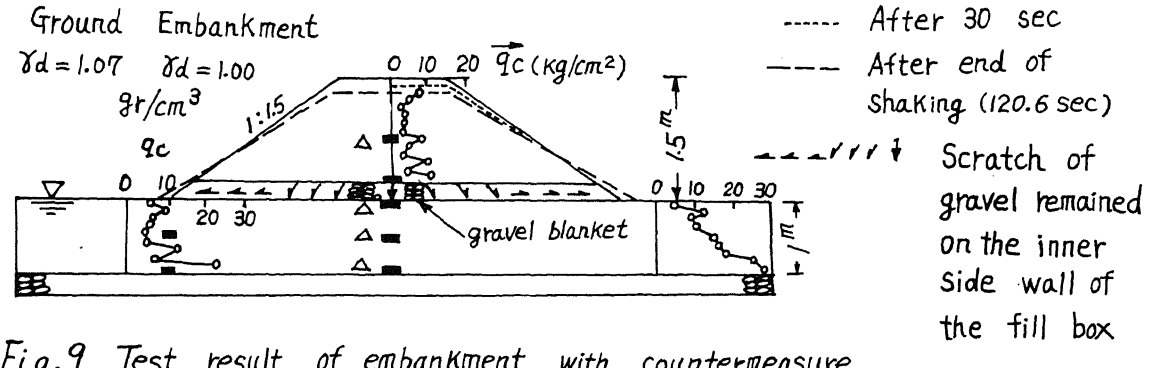

Fig. 9 Test result of embankment with countermeasure (Filling gravel blanket under the embankment)

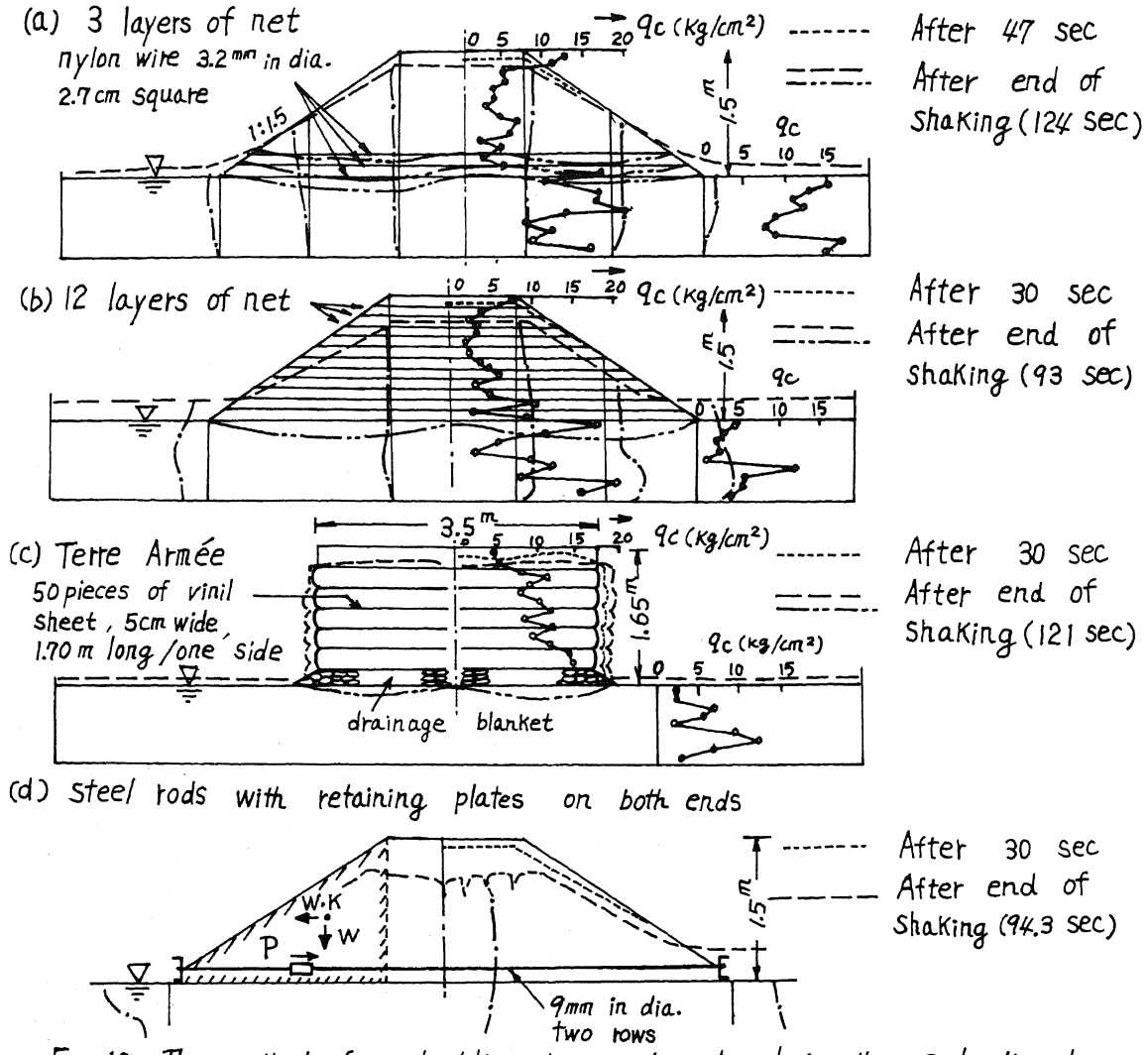

Fig. 10 The method of embedding tensional material in the embankment

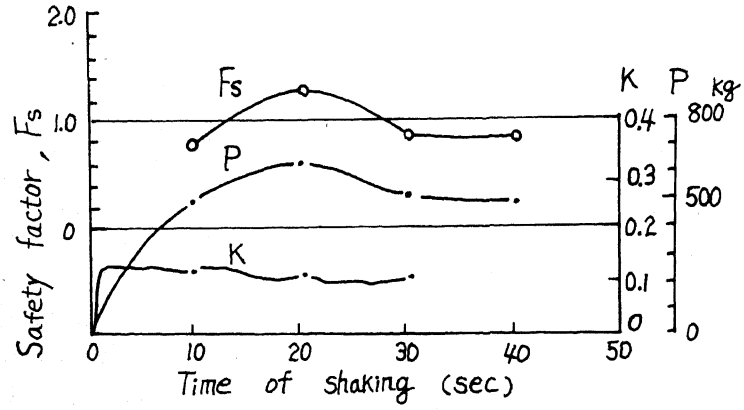

P = measured tensile force acting on steel rods

K = measured horizontal Seismic coefficient

W = weight of triangular block under slope

$$F_s = \frac{P}{W \cdot K}$$

Fig. 11 Measurement of tensile force acting on tensional material

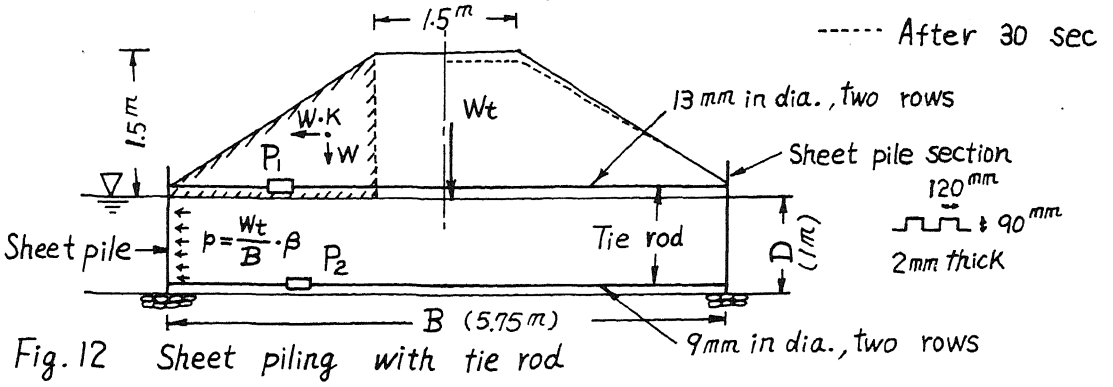

Fig. 12 Sheet piling with tie rod

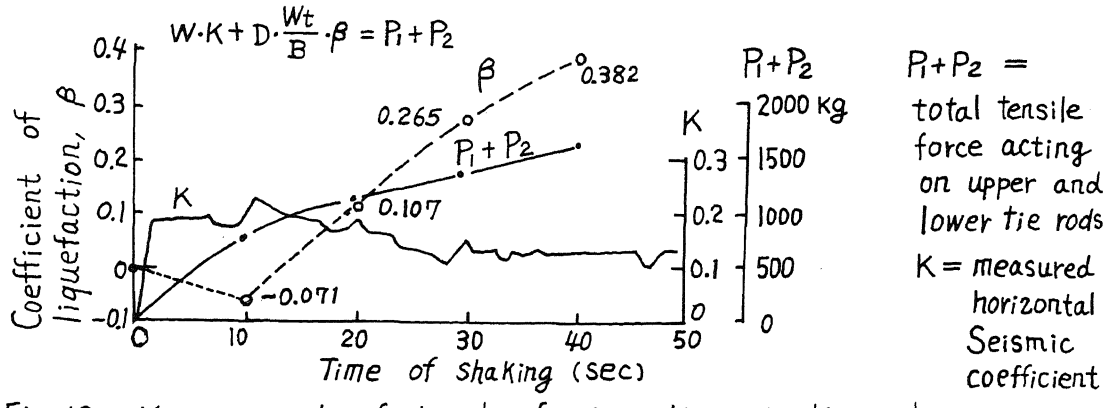

Fig. 13 Measurement of tensile force acting on tie rods

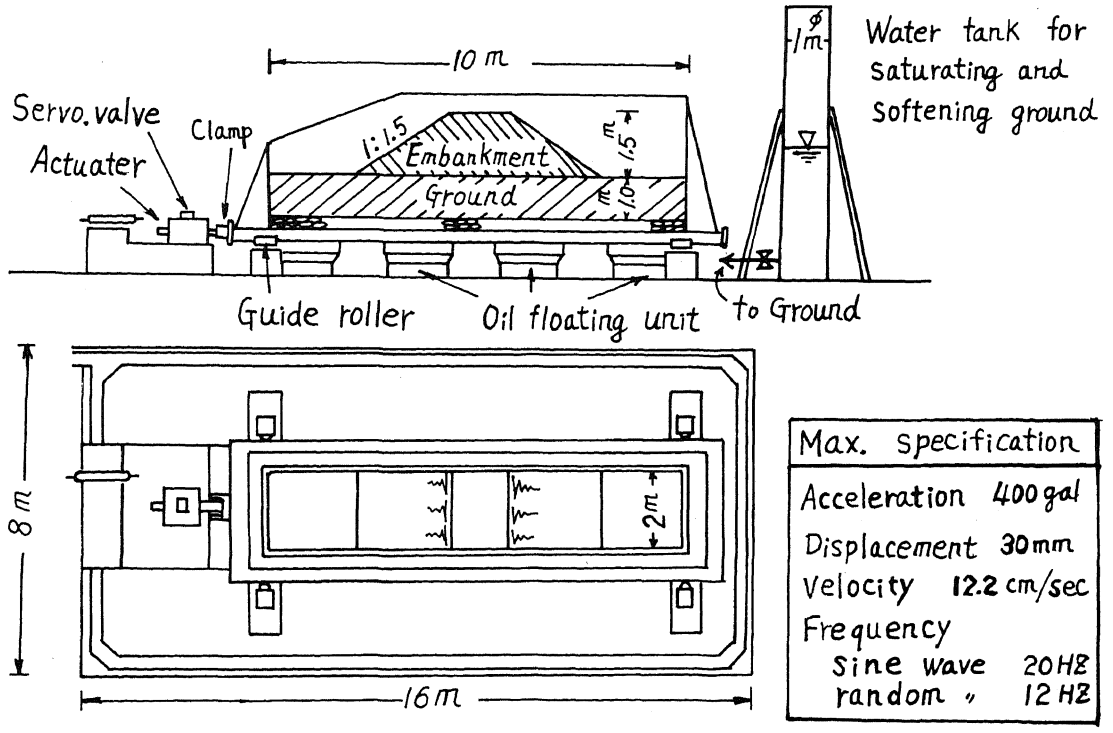

Fig. 14 Layout of the Large-size shaking table at RTRI